

● *Original Contribution*

ULTRASOUND-BASED VESSEL WALL TRACKING: AN AUTO-CORRELATION TECHNIQUE WITH RF CENTER FREQUENCY ESTIMATION

STEIN INGE RABBEN,* STEINAR BJÆRUM,[†] VIDAR SØRHUS[‡] and HANS TORP[§]

*Institute for Surgical Research, University of Oslo, Oslo, Norway; [†]GE Vingmed Ultrasound, Horten, Norway;

[‡]SimSurgery and Interventional Center, National Hospital, Oslo, Norway; [§]Department of Physiology and Biomedical Engineering, Norwegian University of Science and Technology, Trondheim, Norway

(Received 17 January 2000; in final form 16 January 2002)

Abstract—Vessel diameter is related to the distending blood pressure, and is used in estimations of vessel stiffness parameters. The vessel walls can be tracked by integrating wall velocities estimated by ultrasound (US) Doppler techniques. The purpose of this work was to evaluate the performance of the modified autocorrelation estimator when applied on vessel wall motion. As opposed to the conventional autocorrelation method that only estimates the mean Doppler frequency, the modified autocorrelation method estimates both the mean Doppler frequency and the radiofrequency (RF) center frequency. To make a systematic evaluation of the estimator, we performed computer simulations of vessel wall motion, where pulse bandwidth, signal-to-noise ratio (SNR), signal-to-reverberation ratio, packet size and sample volume were varied. As reference, we also analyzed the conventional autocorrelation method and the cross-correlation method with parabolic interpolation. Under the simulation conditions considered here, the modified autocorrelation method had the lowest bias and variance of the estimators. When integrating velocity estimates over several cardiac cycles, the resulting tissue displacement curves might drift. This drift is directly related to the magnitude of the estimator bias and variance. Hence, the modified autocorrelation method should be the preferred choice of method. (E-mail: s.i.rabben@klinmed.uio.no)
© 2002 World Federation for Ultrasound in Medicine & Biology.

Key Words: Ultrasound, Doppler, Vessel wall motion, Echo tracking, Autocorrelation, Cross-correlation.

INTRODUCTION

Noninvasive estimation of arterial wall properties, such as distensibility, compliance and pulse wave velocity, has become increasingly important. Distensibility and compliance can be estimated by combining arterial pressure with vessel diameter measurements (Hansen et al. 1995; Hoeks et al. 1990; Reneman et al. 1986; Tardy et al. 1991), whereas pulse wave velocity can be measured by estimating the time-delay between diameter waveforms recorded simultaneously at two different positions along the vessel (Benthin et al. 1991; Sindberg Eriksen et al. 1985) or by processing the temporal and longitudinal gradients of the change in diameter (Brands et al. 1998). To study heart-vessel interactions, Parker et al. (1988) introduced the wave intensity analysis that reveals the effects of incident and reflected waves on the pressure

and velocity waveforms. Wave intensity analysis can be performed noninvasively by combining vessel diameter measurements with Doppler measurements of blood velocity (Sugawara 1999). Further, to estimate aortic pressure waveforms, investigators (Colan et al. 1985; Aakhus et al. 1993) have calibrated volume-distension (diameter) waveforms recorded at the carotid or the subclavian artery with systolic and diastolic brachial artery pressures.

The vessel diameter can be measured by ultrasound (US) based tracking algorithms. Arndt et al. (1968) described a device that tracked the US echoes from the arterial wall by a threshold detector. The main weakness of this technique is that, because of attenuation, the amplitude of the echoes depends on the distance from the probe to the arterial wall; this distance varies during the cardiac cycle.

Later, Hokanson et al. (1972) presented a phase-locking device that tracked a particular zero crossing within the radiofrequency (RF) signals (vessel wall echoes). This technique improved the radial resolution, down to a few micrometers. The phase-locking technique

Address correspondence to: Dr. Stein I. Rabben, Institute for Surgical Research, National Hospital, 0027 Oslo, Norway. E-mail: s.i.rabben@klinmed.uio.no

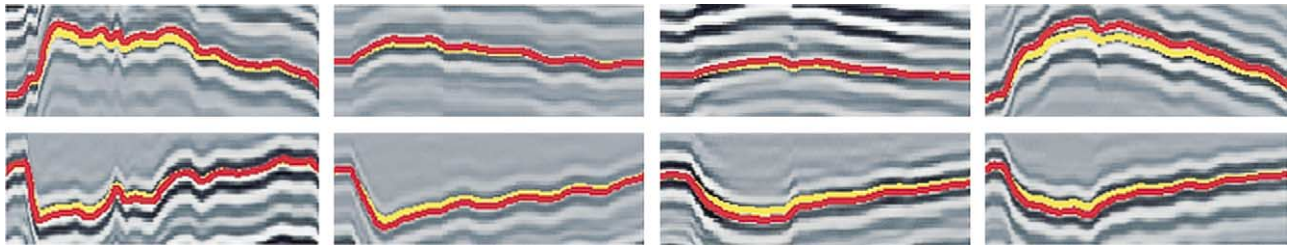


Fig. 1. Examples of wall tracking by the conventional autocorrelation method (yellow lines) and the modified autocorrelation method (red lines). Horizontal axis = time; vertical axis = depth. The tracking was performed on the anterior and posterior walls of the common carotid artery of subjects 31 (left), 41; (middle left), 56 (middle right), and 62 years old (right). The vertical scaling is not identical for the four cases. Note that the conventional autocorrelation method (yellow lines) does not follow the RF lines during all parts of the cardiac cycle. In these examples, RF data were acquired by a 10-MHz linear array probe on a System FiVe ultrasound scanner (GE Vingmed Ultrasound Horten, Norway).

has later been improved by developing digital tracking hardware (Groves et al. 1982), linking the tracking system to B-mode imaging (Imura et al. 1986; Sindberg Eriksen et al. 1985) and combining the tracking system with pressure recordings (Tardy et al. 1991).

As an alternative to the phase-locking technique, Hoeks and coworkers developed a displacement detection system based on conventional autocorrelation. In this system, the average phase over a fixed (Hoeks et al. 1985) or a moving (Hoeks et al. 1990) sample window was used to calculate the displacement. To be unbiased, the conventional autocorrelation estimator requires knowledge of the RF center frequency. Especially for wide bandwidth signals (short pulses), where the RF center frequency is modified by depth-dependent attenuation, the inherent assumption of constant RF center frequency is violated (Fig. 1). Although the estimator bias is small, integration over time may introduce drifting in the tissue displacement curves.

Because cross-correlation is independent of the actual center frequency of the RF signal (Bonnetfous and Pesque 1986), investigators have replaced autocorrelation with RF cross-correlation estimators. The cross-correlation methods estimate the displacement by locating the maximum of the cross-correlation function between two successive RF signals. In general, the location of the maximal cross-correlation does not coincide with the sampling grid and the maximum has to be found by interpolating the sampled cross-correlation function. For example, Moddemeijer (1991) introduced a cross-correlation method that locates the maximum of the sampled cross-correlation function (coarse estimate), fits a parabola to the cross-correlation function around its maximum, and uses the maximum of the parabola as the final estimate, whereas De Jong et al. (1990) developed a cross-correlation method that relies on a Gaussian model of the RF cross-correlation function. One problem with these cross-correlation estimators is that the estimator

bias is nonlinearly dependent on the true displacement. (Hoeks et al. 1993; Lai et al. 1997). Because the incremental displacements of the vessel wall are, on average, larger in the expansion phase (early systole) than in the deflation phase (late systole and diastole), this nonlinearity may lead to drifting when integrating the incremental displacements over several cardiac cycles. Brands et al. (1997) overcome this problem by introducing the complex cross-correlation method, which is an unbiased estimator as long as the RF signal is adequately oversampled.

Because autocorrelation methods have lower sampling rate requirements, it would be favorable to use an autocorrelation technique. Fortunately, the conventional autocorrelation technique can be modified to estimate both the mean Doppler frequency and the RF center frequency inside the observation window (modified autocorrelation method, Fig. 1) (Lai et al. 1997; Loupas et al. 1995; Torp and Kristoffersen 1995). The complex cross-correlation method and the modified autocorrelation method are mathematically identical (Loupas et al. 1995), the difference being that the former is applied on complex RF data, whereas the latter is applied on complex demodulated RF data. In modern US scanners, with digital demodulation, there is no loss in information content, and the two methods should give identical results as long as the complex demodulated RF signal is adequately sampled. Loupas et al. (1995) and Lai et al. (1997) evaluated the modified autocorrelation method on simulations imitating blood flow. However, the signal characteristics of blood flow differs from the signal characteristics of a moving vessel wall.

Hence, the purpose of this work has been to evaluate the bias and variance of the modified autocorrelation method when applied to vessel wall tracking. The evaluation was performed using simulated US data imitating a moving vessel wall. In these simulations, the US imaging process was assumed to be linear and spatially invariant. The US image is then given as a convolution

between the point-spread function and a function representing the acoustical properties of the vessel wall (physical object). The point-spread function included terms accounting for the transmitted US pulse, the frequency-dependent two-way aperture function, frequency-dependent attenuation and Rayleigh scattering. Vessel wall motion was simulated by deforming a cross-section of a vessel wall from time-step to time-step. After an ensemble of 200 image movies was generated, estimator bias and variance were calculated. For reference, we also evaluated the bias and variance of the conventional autocorrelation method (Kasai *et al.* 1985) and the cross-correlation method with parabolic interpolation (Moddemeyer 1991). Finally, we tested the sampling rate requirements of the modified autocorrelation method by varying the sampling rate of the complex demodulated RF data. In this case, we compared the modified autocorrelation method with the complex cross-correlation method (Brands *et al.* 1997).

MATERIALS AND METHODS

The modified autocorrelation method

An RF signal received after pulse transmission is denoted $s_i(z)$, where z is a certain depth from the transducer and corresponds to the elapsed time after pulse transmission (fast-time), and i is the pulse number (slow-time). The RF signal is quadrature-demodulated by applying the following operation:

$$u_i(z) = LPF\{s_i(z)e^{-j2\pi f_m z/c}\}, \quad (1)$$

where LPF represents a low-pass filter, $j = \sqrt{-1}$, f_m is the demodulation frequency, and c is the speed of sound. Note that $u_i(z)$ is a complex signal with in-phase (real) and quadrature (imaginary) components (IQ data).

In the conventional autocorrelation method, the displacement in the beam direction is estimated as (Kasai *et al.* 1985):

$$\widehat{\Delta z} = \frac{1}{2} \frac{\angle \hat{R}(0, 1)}{2\pi} \frac{c}{f_m} \quad (2)$$

where \angle denotes phase angle, and $\hat{R}(0, 1)$ is the complex-valued autocorrelation estimate of $u_i(z)$ at a certain depth z . The conventional autocorrelation method is unbiased, provided that the demodulation frequency f_m is equal to the center frequency of the received RF signal. However, frequency-dependent attenuation causes variations in the RF center frequency.

In the modified autocorrelation method, the RF center frequency is estimated as (Lai *et al.* 1997; Loupas *et al.* 1995; Torp and Kristoffersen 1995):

$$\hat{f}_0 = f_m + \frac{\angle \hat{R}(1, 0)}{2\pi} f_s \quad (3)$$

where f_s is the sampling frequency, and $\hat{R}(1, 0)$ is the estimate of the complex-valued autocorrelation of $u_i(z)$ in the range direction. The last term on the right hand side of eqn (3) is an estimate of the mean frequency of the quadrature-demodulated signal, and corresponds to the deviation between the demodulation frequency f_m and the RF center frequency. In the modified autocorrelation method, the demodulation frequency used in the conventional autocorrelation method, eqn (2), is replaced by the estimated RF center frequency, eqn (3):

$$\widehat{\Delta z} = \frac{1}{2} \frac{\angle \hat{R}(0, 1)}{2\pi} \frac{c}{\hat{f}_0} \quad (4)$$

In this study, the sample mean estimator was used for determining \hat{R} :

$$\hat{R}(m', n') = \frac{1}{M - m'} \frac{1}{N - n'} \sum_{m=0}^{M-m'-1} \sum_{n=0}^{N-n'-1} u_n(m) * u_{n+n'}(m + m'), \quad m' \geq 0, n' \geq 0, \quad (5)$$

where m' and n' are the spatial and temporal lags, and $M \times N$ is the estimation window.

Simulation model

This section describes the simulation model imitating a moving vessel wall.

Image formation. The US imaging process was assumed to be linear and spatially invariant. The latter assumption is appropriate in the transmit focal zone. The US image g_i is then given as a convolution between the point spread function h and a function f_i representing the acoustical properties of the object. For a linear scan, this is described by:

$$g_i(x, z) = \int h(x_1, y_1, z_1) f_i(x - x_1, -y_1, z - z_1) dx_1 dy_1 dz_1, \quad (6)$$

where x , y and z are the coordinates in the lateral, elevation and range directions, respectively, and subscript i denotes image number. Assume further that $f(x, y, z) = \tilde{f}(x, z)$ within the beam (*i.e.*, in the region where $h(x, y, z) \neq 0$). For blood vessels, this will be the case when the y direction corresponds to the longitudinal direction of the vessel, and the x - z plane corresponds to

the cross section of the vessel. Equation (6) can then be written as:

$$g_i(x, z) = \int \tilde{f}_i(x - x_1, z - z_1) \int h(x_1, y_1, z_1) dy_1 dx_1 dz_1. \quad (7)$$

For a rectangular aperture, the point spread function is separable in the x and y directions (*i.e.*, $h(x, y, z) = h_{xz}(x, z) h_{yz}(y, z)$), and

$$\int h(x, y, z) dy = h_{xz}(x, z) \int h_{yz}(y, z) dy = \tilde{h}(x, z). \quad (8)$$

Inserting this into eqn (7) gives:

$$g_i(x, z) = \int \tilde{h}(x_1, z_1) \tilde{f}_i(x - x_1, z - z_1) dx_1 dz_1, \quad (9)$$

which is a 2-D convolution. In the frequency domain, this corresponds to:

$$G_i(k_x, k_z) = F_i(k_x, k_z) \cdot H(k_x, k_z), \quad (10)$$

where k denotes wave numbers.

Point spread function. In the simulations, the point spread function contained the following terms:

$$H(k_x, k_z) = A(k_x, k_z) \cdot P(k_z) \cdot k_z^2 \cdot \alpha(k_z), \quad (11)$$

where A is the frequency representation of the two-way aperture, P is the Fourier transform of the transmitted US pulse, and α accounts for frequency-dependent attenuation. The third term on the right-hand side represents Rayleigh scattering. We assumed P to be Gaussian-shaped, with center frequency f_0 and bandwidth B defined as twice the RMS bandwidth (*i.e.*, -17 -dB bandwidth). The aperture function A was calculated as $A_{tx} * A_{rx}$, where $*$ denotes 1-D convolution in the k_x direction. The transmitter and receiver apertures (A_{tx} and A_{rx}) were given by:

$$A_{rx}(k_x, k_z) = A_{tx}(k_x, k_z) = \begin{cases} \frac{4\pi}{k_x} F_{\#}, & |k_x| \leq \frac{k_z}{4F_{\#}} \\ 0, & |k_x| > \frac{k_z}{4F_{\#}} \end{cases} \quad (12)$$

where $F_{\#}$ is the F number. Rectangular apodization was, hence, used.

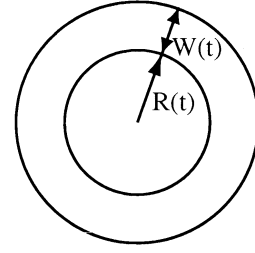


Fig. 2. Cross-section of a blood vessel. $R(t)$ = inner radius; $W(t)$ = wall thickness.

Object generation. We wanted the object movie $f_i(x, z)$ to represent a cross-section of a blood vessel with time-varying inner radius $R(t)$ and wall thickness $W(t)$ (Fig. 2).

If we assume a uniform deformation in the radial direction of the blood vessel, the motion of a material point within the vessel wall is described by:

$$r(t, x, z) = \frac{W(t)}{W(0)} [r(0, x, z) - R(0)] + R(t), \quad (13)$$

where r is the radial coordinate of a polar coordinate system with origin in the center of the vessel.

In the first object-frame f_1 , the pixels within the wall were given values that fluctuated randomly (Gaussian distribution, with an SD of 25) around a mean value of 200, whereas the pixels representing blood were set to zero. The blood signal component was neglected because scattering caused by blood is much lower than scattering caused by tissue. The intensity variation of the pixels within the wall mimics the inherent variation of mass density and compressibility in soft tissue causing scattering of the US pulse.

Because the object is defined on a fixed grid given by the pixel positions and the blood vessel experiences subpixel deformation, we generated the object movie by applying the following algorithm at each time-step.

1. Transform the pixel positions to polar coordinates.
2. Calculate the positions that each pixel of frame f_i had prior to deformation by applying the following formula:

$$r_1(x, z) = \frac{W_1}{W_i} [r_i(x, z) - R_i] + R_1 \quad (14)$$

3. Transform the calculated positions back to Cartesian coordinates.
4. Interpolate the first frame f_1 at the calculated positions (spline interpolation) and assign the interpolated values to the corresponding pixels of frame f_i .

The pixel size of the object-frames was $19.25 \mu\text{m}$. In the range direction, this corresponds to a sampling

frequency of 40 MHz. Before interpolation, the first object-frame (f_1) was smoothed by an eighth order spatial Butterworth filter with a 3-dB cut-off frequency of 1558 m^{-1} . In the range direction, this corresponds to 12 MHz. The spatial filtering of the first object-frame had to be done to avoid aliasing effects caused by the infinite bandwidth of the spline-based interpolation filter. An ideal interpolation filter, with finite bandwidth, cannot be used because it requires an infinite number of sampling points. The cut-off frequency of the spatial filter was set to 1558 m^{-1} (12 MHz) because this is higher than the pass band of the image filter (point spread function). The spatial filtering of the object should, therefore, not affect the simulated RF data.

To reduce computation time, only the upper part of the cross-section of the vessel was generated (Fig. 3A). Note that this represents a vessel with blood on each side of the wall. However, this is often the case for a portion of the common carotid artery where the internal jugular vein is positioned anterior to the artery.

RF data generation. A block diagram of the simulations is shown in Fig. 4. Ultrasound RF data were generated by Fourier transforming the objects, applying eqn (10) and inverse Fourier-transforming the resulting frequency-domain data. In each image $g_i(x, z)$, the RF signal at the middle of the vessel (lateral position x_0) was selected (M-mode extractor, Fig. 4). The selected RF signals were organized in an array (RF M-mode). Thermal noise was simulated by adding white Gaussian noise to all sample points in the ultrasound RF M-mode ($n_i(z)$), whereas stationary reverberations were simulated by generating one Gaussian noise vector ($w(z)$) and adding this to all the lines of the RF M-mode. The SNR and the signal-to-reverberation ratio (SRR) were defined as the power of the tissue signal divided by the power of the noise and reverberations, respectively. The total signal $s'_i(z)$, including noise and stationary reverberations, was quadrature-demodulated, eqn (1), and low-pass filtered with a bandwidth matched to the pulse bandwidth B (right part of Fig. 4). This was done to mimic the processing of the modern US scanner, where the SNR is improved by using a receiver filter matched to the bandwidth of the RF signal (Kristoffersen 1986). Moreover, by specifying the SNR before filtering, the simulation model imitates a situation with constant thermal index. The filtered data were 1. modulated up to RF data ($s_i(z)$) and used by the cross-correlation methods (CC) or 2. down-sampled to 10 MHz ($u_i(z)$) and used by the auto-correlation methods (AC). Table 1 shows the parameters common to all simulations. All the simulations were performed by using Matlab v6.0 (MathWorks Inc., Natick, Massachusetts).

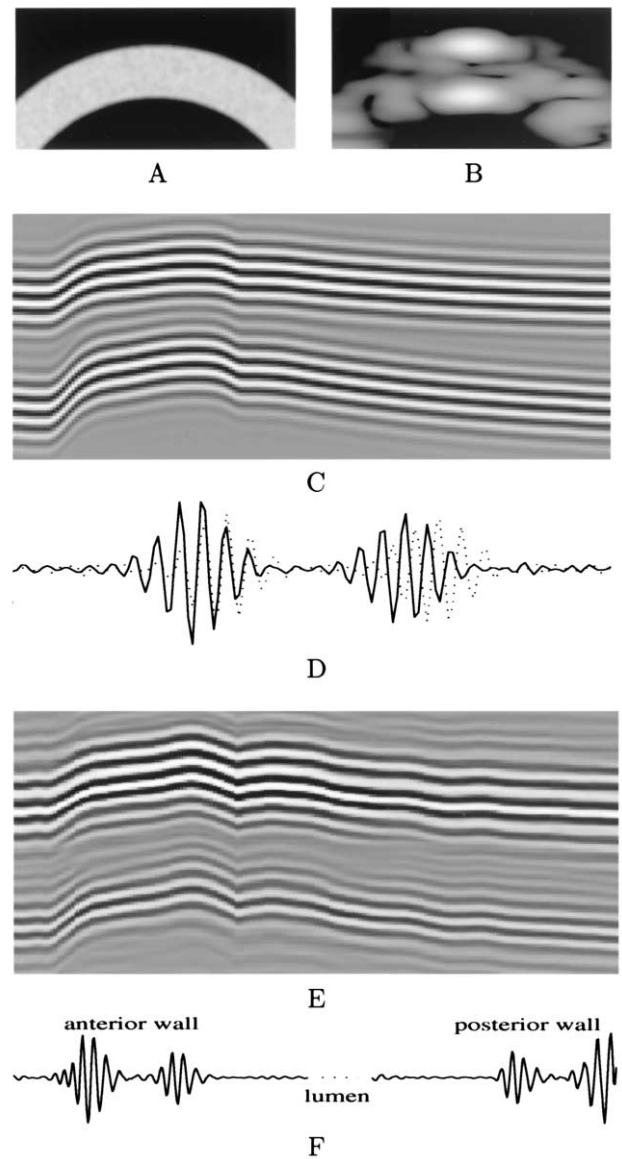


Fig. 3. (A) Simulated object $f_i(x, z)$; (B) simulated US image $g_i(x, z)$; (C) simulated RF grey-scale M-mode (extracted from the middle of the the US image). (D) Simulated RF signal before (—) and after (⋯) the wall has moved. (E) RF grey-scale M-mode of the anterior wall of the carotid artery of a 62-year-old hypertensive subject. (F) RF signal from the same subject. Note that a portion of the RF signal has been removed (dotted line).

Physiological wall-motion simulations

To imitate physiological wall motion, we generated a series of object frames (object movie) where the radius and wall thickness were changed according to measurements from the common carotid artery of a 62-year-old subject (right panels, Fig. 1). In this subject, the mean radius was 2.9 mm and the mean wall thickness was 0.93 mm. The object movie contained 97 frames covering one

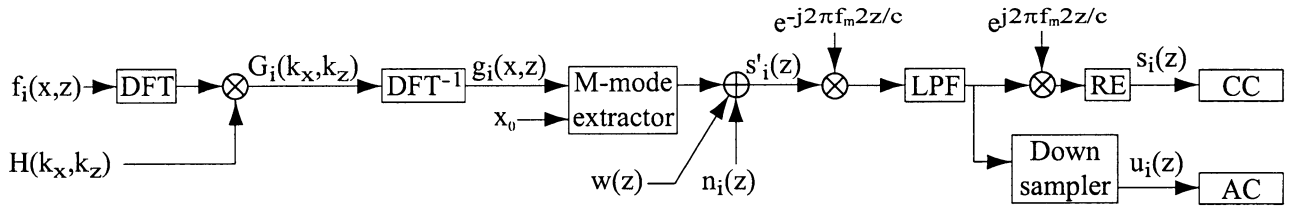


Fig. 4. Block diagram of the signal simulation. The object $f_i(x, z)$ is Fourier-transformed and multiplied by the point spread function $H(k_x, k_z)$. The resulting frequency representation ($G_i(k_x, k_z)$) is inverse Fourier-transformed. From each image $g_i(x, z)$, the RF signal at the lateral position x_0 is selected and organized in an RF M-mode. Thermal noise $n_i(z)$ and stationary reverberations $w(z)$ are added, and the resulting signal $s'_i(z)$ is quadrature-demodulated and low-pass filtered. The filtered data was 1. modulated up to RF data ($s_i(z)$) and used by the cross-correlation methods (CC) or 2. down-sampled to 10 MHz ($u_i(z)$) and used by the autocorrelation methods (AC). DFT = digital Fourier transform; LPF = low-pass filter; RE = real operator.

cardiac cycle. Ultrasound RF data were generated from the object movie and the wall was tracked by the different displacement estimators. The parameter settings were as shown in Table 2.

Evaluation of estimator bias and variance

To obtain estimates of estimator bias and variance, we generated an ensemble of 200 object movies, each containing 80 frames. In the first frame, the radius was set to 3 mm, whereas the wall thickness was set to 0.9 mm. From frame to frame, the vessel radius was increased by 0.025λ , where λ is the transmitted wavelength (*i.e.*, $\lambda = c/f_0$). This way, up to 8000, 4000 and 2000 displacement estimates were generated for packet sizes of 2, 4 and 8 pulses, respectively. Such a high number of estimates ensured reliable statistics. The parameter settings (shown in Table 3) were chosen according to what is common in tissue Doppler imaging.

RESULTS

Physiological wall-motion simulations

An example of the simulation output is shown in Fig. 3A–D. For comparison, RF data recorded from a 62-year-old hypertensive subject are shown in Fig. 3E–F. The RF data were acquired by a 10-MHz linear array probe on a System FiVe US scanner (GE Vingmed Ultrasound, Horten, Norway).

Table 1. Parameters common to all simulations

Parameter	Symbol	Value	Unit
Speed of sound	c	1540	m/s
Pulse center frequency	f_0	8	MHz
Sampling frequency	f_s	40	MHz
Frequency-dependent attenuation	α	2	dB/MHz
F-number (transmit and receive)	$F_{\#}$	4.5	–
Demodulation frequency	f_m	7.75	MHz

Figure 5 shows examples of wall tracking. In Fig. 5A, B and C, the pulse bandwidths were $0.25 f_0$, $0.5 f_0$ and $0.75 f_0$, respectively. The conventional autocorrelation method overestimated wall excursion in A, but underestimated the wall excursion in C. However, when comparing the wall position at the start and end of the cardiac cycle, we see little global drifting. The cross-correlation method with parabolic interpolation drifted slightly in all three cases. The modified autocorrelation method gave negligible drifting in all conditions.

Evaluation of estimator bias and variance

Packet size. Figure 6 shows the bias and SD as a function of displacement for packet sizes equal to 2, 4 and 8 pulses. The fixed parameters for these simulations were: pulse bandwidth $0.5 f_0$, SNR 15 dB, SRR 25 dB and sample volume 2.5 wavelengths. As expected, Fig. 6 shows that the SD of the estimators was inversely related to the packet size. For all packet sizes, the conventional autocorrelation method had the highest SD, whereas the modified autocorrelation method and cross-correlation method had SDs in the same range. The modified autocorrelation method had the lowest bias. The bias of the estimators was not much affected by the packet size.

Sample volume. Figure 7 shows the bias and SD as a function of displacement for sample volumes equal to

Table 2. Parameter settings for the physiological wall-motion simulations

Parameter	Symbol	Value(s)	Unit
Pulse bandwidth	B	0.25, 0.5, 0.75	f_0
SNR	SNR	25	dB
Sample volume	M	2.5	λ
Packet size	N	2	lines

λ is the transmitted wavelength (*i.e.*, $\lambda = c/f_0$). Reverberation noise was not added to the RF data in these simulations.

Table 3. Parameter settings for bias and variance estimations

Parameter	Symbol	Values	Unit
Displacements	Δz	0.025, 0.05, . . . , 0.225	λ
Pulse bandwidth	B	0.25, 0.5, 0.75	f_0
Signal-to-noise ratio	SNR	5, 15, 25	dB
Signal-to-reverberation ratio	SRR	5, 25, ∞	dB
Sample volume	M	1, 2.5, 4	λ
Packet size	N	2, 4, 8	lines

1, 2.5 and 4 wavelengths. The fixed parameters for these simulations were: pulse bandwidth $0.5 f_0$, SNR 15 dB, SRR 25 dB and packet size 4 pulses. Figure 7 shows that the performance of the autocorrelation methods did not depend much on the size of the sample volume, whereas the cross-correlation method became unreliable for the shortest sample volume (1λ). This indicates that the cross-correlation method probably detects false peaks for the shortest sample volume. The reason might be that the variance of the sample mean correlation estimator, eqn (5), increases when the correlation lag is large compared with the size of the estimation window. For the other sample volumes, the modified autocorrelation and the cross-correlation methods had SDs in the same range.

Signal-to-noise ratio. Figure 8 shows the bias and SD as a function of displacement for SNRs equal to 5, 15 and 25 dB. The fixed parameters for these simulations were: pulse bandwidth $0.5 f_0$, SRR 25 dB, packet size 4 pulses and sample volume 2.5 wavelengths. As expected, for all estimators, the SD increased with the noise level. The difference in SD between the conventional and the modified autocorrelation methods was quite small for an SNR of 5 dB. This indicates that the benefit of estimating the RF center frequency is marginal under heavy noise conditions. However, the bias, which is the most important estimator property in vessel wall tracking, was not much affected by the noise level.

Be aware that, in our simulation model, we added thermal noise before applying a receiver filter matched to the pulse bandwidth. This means that the effective SNR (SNR after filtering) depends on the ratio between the pulse bandwidth and the noise bandwidth. In the simulations of Fig. 8, with a pulse bandwidth of 4 MHz and a noise bandwidth of 20 MHz, the receiver filter improves the SNR by 7 dB ($10 \log(4/20) = -7$ dB). The three columns of Fig. 8, therefore, correspond to an effective SNR of 12, 22 and 32 dB.

Signal-to-reverberation ratio. Figure 9 shows the bias and SD as a function of displacement for SRRs equal to 5, 25 and ∞ dB. The fixed parameters for these simulations were: pulse bandwidth $0.5 f_0$, SNR 15 dB, packet size 4 pulses and sample volume 2.5 wavelengths. For all meth-

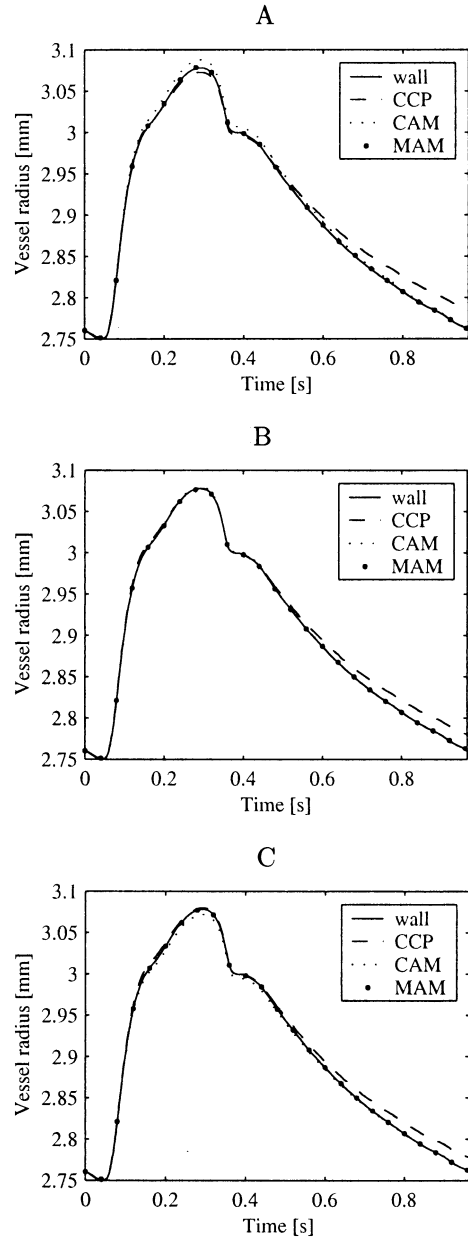


Fig. 5. Examples of tracking when using data from the physiological wall-motion simulations. The parameter settings are given in Table 2. The pulse bandwidth was (A) $0.25 f_0$, (B) $0.5 f_0$ and (C) $0.75 f_0$, respectively. (—) True vessel wall; (---) cross-correlation with parabolic interpolation (CCP); (⋯) conventional autocorrelation (CAM); (•••) modified autocorrelation (MAM).

ods, both the bias and SD were affected by changing the reverberation level. At SRR of 5 dB, all estimators became unreliable. Figure 9 also shows that an SRR of 25 dB is similar to having no reverberations (∞ dB).

Pulse bandwidth. Figure 10 shows the bias and SD as a function of displacement for pulse bandwidths equal

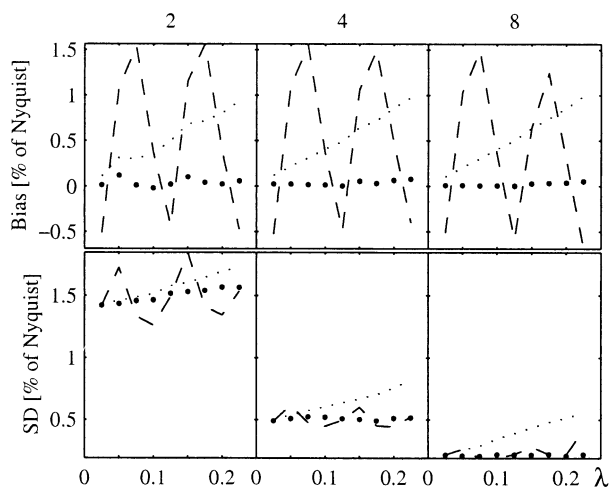


Fig. 6. Bias and SD as a function of displacement for packet sizes equal to 2, 4 and 8 pulses. (---) Cross-correlation with parabolic interpolation; (...) conventional autocorrelation; (●●●) modified autocorrelation.

to 0.25, 0.5 and 0.75 f_0 . These pulse bandwidths correspond to pulse lengths of approximately 10.2, 5.1 and 3.4 wavelengths, respectively. The fixed parameters for these simulations were: SNR 15 dB, SRR 25 dB, packet size 4 pulses and sample volume 2.5 wavelengths. The biases and the SDs of the modified autocorrelation method and the cross-correlation method did not change much for the three alternative pulse lengths. The bias of the conventional autocorrelation method changed substantially for the three alternative pulse lengths. The reason is that the same demodulation frequency was used

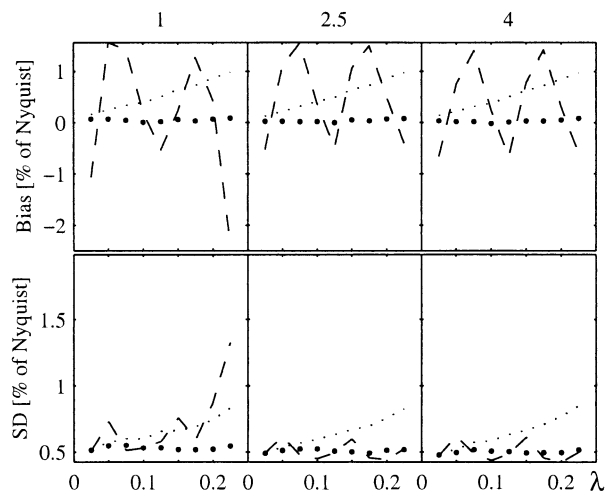


Fig. 7. Bias and SD as a function of displacement for sample volumes equal to 1, 2.5 and 4 wavelengths. Line styles described in the legend for Fig. 6.

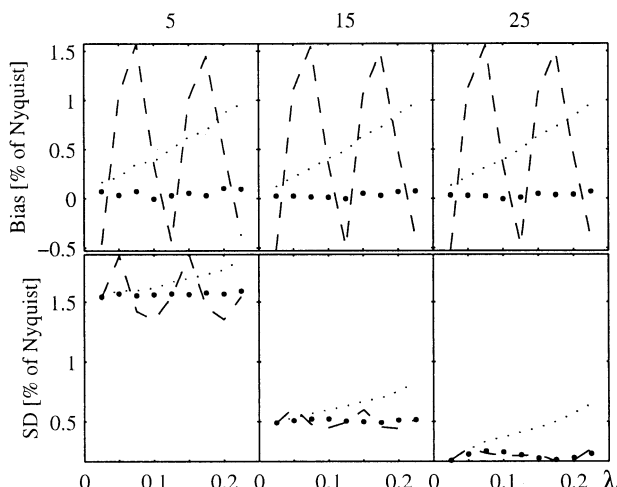


Fig. 8. Bias and SD as a function of displacement for SNRs equal to 5, 15 and 25. Line styles described in legend for Fig. 6.

in all three cases. As expected, the SD of the conventional autocorrelation method increased with decreasing pulse lengths. The reason is that the shortest pulse gives the fastest decorrelation.

Note that the effective SNR (SNR after filtering) depends on the ratio between the pulse bandwidth and the noise bandwidth. Therefore, in the simulations of Fig. 10, with pulse bandwidths of 2, 4 and 6 MHz and a noise bandwidth of 20 MHz, the effective SNR is 25, 22 and 20.2 dB, respectively.

IQ sampling rate. Figure 11 shows the bias and SD of the modified autocorrelation method (...) applied on the complex demodulated RF data that has been down-

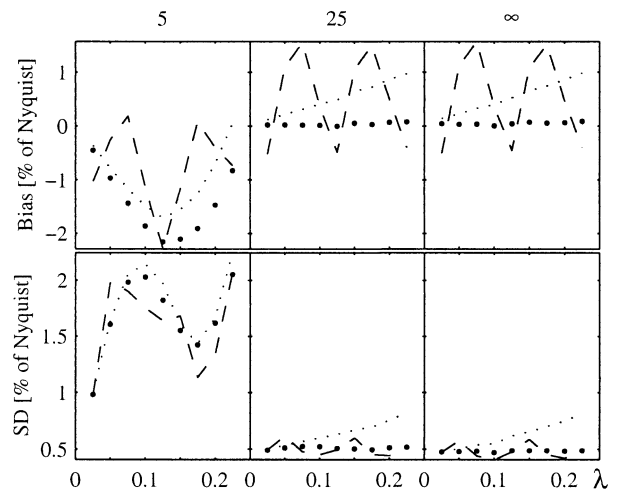


Fig. 9. Bias and SD as a function of displacement for SRRs equal to 5, 25 and ∞ . Line styles described in legend for Fig. 6.

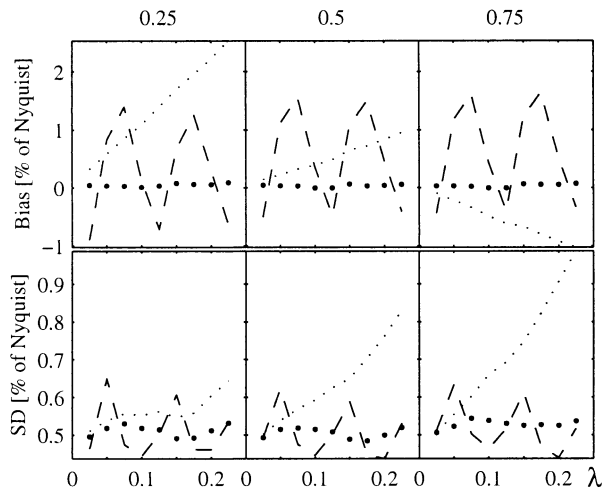


Fig. 10. Bias and SD as a function of displacement for pulse bandwidths equal to 0.25, 0.5 and 0.75 f_0 . Line styles described in legend for Fig. 6.

sampled from 40 MHz to 10, 6.7 and 4 MHz. For reference, Fig. 11 also shows the bias and SD of the complex cross-correlation method (—) applied on the original RF data (sampling frequency of 40 MHz). The fixed parameters for these simulations were: SNR 15 dB, SRR 25 dB, packet size 4 pulses, sample volume 2.5 wavelengths and pulse bandwidth 0.5 f_0 . Figure 11 illustrates that the modified autocorrelation method and the complex cross-correlation method give identical results as long as the complex demodulated RF signal is adequately oversampled. At the critical sampling rate (pulse bandwidth = 0.5 f_0 = 4 MHz), the modified autocorrelation method became unreliable.

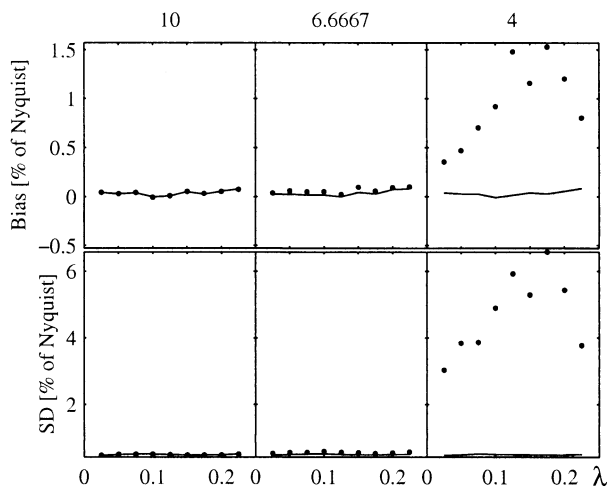


Fig. 11. Bias and SD of modified autocorrelation method (· · ·) for sampling rates of 10, 6.7 and 4 MHz; (—) complex cross-correlation (sampling rate: 40 MHz).

DISCUSSION

Displacement estimators based on 1. the modified autocorrelation method (Lai *et al.* 1997; Loupas *et al.* 1995; Torp and Kristoffersen 1995), 2. the conventional autocorrelation method (Kasai *et al.* 1985) and 3. the cross-correlation method with parabolic interpolation (Moddemeijer 1991) were evaluated by calculating bias and variance from computer simulations of a moving vessel wall. To make a systematic comparison of the estimators, we varied the pulse bandwidth, SNR, SRR, packet size and sample volume. Under the simulation conditions considered in this study, the modified autocorrelation method had the lowest bias and variance of the three methods.

Simulation model

Figure 3A–D shows an example of the US simulations. Compared to measured RF data from a hypertensive subject (Fig. 3E–F), there are a number of similarities. As in the measured RF data, the main echoes in the simulated RF data are related to the blood-to-tissue transitions of the vessel wall. The amplitude of the echoes is partly related to the interaction between the point spread function and the vessel wall curvature. Low curvatures give stronger specular reflections than high curvatures. In both the simulated and the measured RF signals (Fig. 3D and F), the first echo has a higher amplitude than the second echo, the reason being that the outer edge has a lower curvature than the inner edge. Both the measurements and the simulations illustrate the effects of wall thinning. When the distance between the two main echoes changes during the cardiac cycle, the two echoes interfere. Between the two main echoes, the phase of the RF signal changes abruptly, and RF lines suddenly appear or disappear (Fig. 3C and E).

The main purpose of the simulation models of former studies (Lai *et al.* 1997; Loupas *et al.* 1995) have been to evaluate blood velocity estimation. In blood flow, the scatters have a rather large velocity distribution. Hence, the estimators have been evaluated for a range of velocity distributions. In tissue motion, there is a much smaller velocity distribution around the mean velocity. In our simulation model, we only specify the change of the vessel radius and wall thickness from time-step to time-step and, thereby, do not specify a velocity distribution. However, the change in curvature of the outer and inner edges implicitly gives a phase distribution in the simulated RF signal. The different scatters, within the point spread function, will move with different velocities (in the z direction) because of the curvature of the vessel wall.

Drifting

In vessel wall tracking, the tissue displacement curves are obtained by integrating the instantaneous displacement estimates. However, the tissue displacement curves may drift because of the accumulative effects of the estimator bias and variance. If N is the number of time-steps in the integration, the SD of the displacement curves increases with a factor of \sqrt{N} , whereas the bias of the tissue displacement curves increases with a factor of N . Because the estimator bias and SD are in the same range (Figs. 6–10), this means that, after some time-steps, the bias dominates over SD.

When discussing drifting, it is constructive to differentiate global from local drifting. We define global drifting as the distance between the true and the estimated wall positions after tracking of one cardiac cycle. By local drifting, we mean the instantaneous distance from the true and the estimated wall positions during the cardiac cycle. Figure 1 shows tracking examples with local drifting but no global drifting (yellow lines), whereas Fig. 5 shows simulations with both local and global drifting.

Global drifting is typically seen when using a displacement estimator with a bias that is nonlinearly dependent on the true displacement (*e.g.*, the cross-correlation method) (Figs. 6–10). Because the incremental displacements of the vessel wall are, on average, larger in the expansion phase (early systole) than in the deflation phase (late systole and diastole), this nonlinearity may lead to drifting when integrating the incremental displacements over one cardiac cycle. Lai et al. (1997) have shown that the bias of the cross-correlator with parabolic interpolation decreases when the sampling frequency is increased from 4 times f_0 to 8 times f_0 . However, at a sampling frequency of 8 times f_0 , they still observed estimation bias.

For the conventional autocorrelation method, the bias is proportional to the true displacement (Figs. 6–10). The displacement estimation error will, in this case, be proportional to the true displacement and local drifting will be observed (Figs. 1 and 5). The bias of the conventional autocorrelation method depends on the difference between the chosen demodulation frequency f_m and the instantaneous RF center frequency. Because the instantaneous RF center frequency is affected by frequency-dependent attenuation (Duck 1990), the local drifting may become substantial and the algorithm may, in some cases, track out of the wall and into the vessel cavity. In the US recordings from the four subjects (Fig. 1), the -17 -dB bandwidth of the RF signals were in the range of 4–5 MHz. In such wide band signals, the center frequency of the received signal will be affected by frequency-dependent attenuation.

Sampling rate requirements

Figure 11 illustrates that the modified autocorrelation method and the complex cross-correlation method give identical results, as long as the complex demodulated RF signal is adequately sampled. In the simulations shown in Figs. 6–10, we down-sampled the complex demodulated RF data to 10 MHz. In these cases, the complex cross-correlation method and the modified autocorrelation method give identical results. However, we see from the middle panels of Fig. 11 that a sampling rate of 6.7 MHz gives small differences between the complex cross-correlation method and the modified autocorrelation method. At critical sampling, where the sampling rate equals the pulse bandwidth, the modified autocorrelation method became unreliable. A sampling frequency of 4 times f_0 (= 32 MHz) is adequate for excluding the bias of the complex cross-correlation method (Brands et al. 1997). Figure 11 shows that the modified autocorrelation method requires a sampling frequency of 7–10 MHz.

CONCLUSION

Under the simulation conditions considered here, the modified autocorrelation method had lower bias and variance than the conventional autocorrelation method and the cross-correlation method with parabolic interpolation. When integrating velocity estimates over several cardiac cycles, the resulting tissue displacement curves might drift. This drift is directly related to the magnitude of the estimator bias and variance. Hence, the modified autocorrelation method should be the preferred choice of method.

Acknowledgements—This study was supported by Program for Medical Technology at the Norwegian University of Science and Technology. The authors thank Andreas Heimdal for helpful discussions about the computer simulations.

REFERENCES

- Aakhus S, Torp H, Haugland T, Hatle L. Non-invasive estimates of aortic root pressures: External subclavian arterial pulse tracing calibrated by oscillometrically determined brachial arterial pressures. *Clin Physiol* 1993;13:573–586.
- Arndt JO, Klauske J, Mersch F. The diameter of the intact carotid artery in man and its change with pulse pressure. *Pflugers Arch Gesamte Physiol Menschen Tiere* 1968;301:230–240.
- Benthin M, Dahl P, Ruzicka R, Lindstrom K. Calculation of pulse-wave velocity using cross correlation—effects of reflexes in the arterial tree. *Ultrasound Med Biol* 1991;17:461–469.
- Bonnefous O, Pesque P. Time-domain formulation of pulse doppler ultrasound and blood velocity estimation by cross correlation. *Ultrasound Imaging* 1986;8:73–85.
- Brands PJ, Hoeks AP, Ledoux LA, Reneman RS. A radio frequency domain complex cross-correlation model to estimate blood flow velocity and tissue motion by means of ultrasound. *Ultrasound Med Biol* 1997;23:911–920.
- Brands PJ, Willigers JM, Ledoux LA, Reneman RS, Hoeks AP. A noninvasive method to estimate pulse wave velocity in arteries locally by means of ultrasound. *Ultrasound Med Biol* 1998;24:1325–1335.

- Colan SD, Borow KM, Neumann A. Use of the calibrated carotid pulse tracing for calculation of left ventricular pressure and wall stress throughout ejection. *Am Heart J* 1985;109:1306–1310.
- De Jong PGM, Arts T, Hoeks APG, Reneman RS. Determination of tissue motion velocity by correlation interpolation of pulsed ultrasonic echo signals. *Ultrasound Imaging* 1990;12:84–98.
- Duck FA. Physical properties of tissue. A comprehensive reference book. London: Academic Press, 1990.
- Groves DH, Powalowski T, White DN. A digital technique for tracking moving interfaces. *Ultrasound Med Biol* 1982;8:185–190.
- Hansen F, Mangell P, Sonesson B, Lanne T. Diameter and compliance in the human common carotid artery—variations with age and sex. *Ultrasound Med Biol* 1995;21:1–9.
- Hoeks AP, Arts T, Brands PJ, Reneman RS. Comparison of the performance of the RF cross correlation and Doppler autocorrelation technique to estimate the mean velocity of simulated ultrasound signals. *Ultrasound Med Biol* 1993;19:727–740.
- Hoeks AP, Brands PJ, Smeets FA, Reneman RS. Assessment of the distensibility of superficial arteries. *Ultrasound Med Biol* 1990;16:121–128.
- Hoeks AP, Ruissen CJ, Hick P, Reneman RS. Transcutaneous detection of relative changes in artery diameter. *Ultrasound Med Biol* 1985;11:51–59.
- Hokanson DE, Mozersky DJ, Summer DS, Strandness DE. A phase-locked echo tracking system for recording arterial diameter changes in vivo. *J Appl Physiol* 1972;32:728–733.
- Imura T, Yamamoto K, Kanamori K, Mikami T, Yasuda H. Non-invasive ultrasonic measurement of the elastic properties of the human abdominal aorta. *Cardiovasc Res* 1986;20:208–214.
- Kasai C, Namekawa K, Koyano A, Omoto R. Real-time two-dimensional blood flow imaging using an autocorrelation technique. *IEEE Trans Sonics Ultrason* 1985;SU-32:458–463.
- Kristoffersen K. Optimal receiver filtering in pulsed Doppler ultrasound blood measurements. *IEEE Trans Ultrason Ferroelec Freq Control* 1986;33:51–58.
- Lai X, Torp H, Kristoffersen K. An extended autocorrelation method for estimation of blood velocity. *IEEE Trans Ultrason Ferroelec Freq Control* 1997;44:1332–1342.
- Loupas T, Powers JT, Gill RW. An axial velocity estimator for ultrasound blood flow imaging, based on a full evaluation of the doppler equation by means of a two-dimensional autocorrelation approach. *IEEE Trans Ultrason Ferroelec Freq Control* 1995;42:672–688.
- Moddemeijer R. On the determination of the position of extrema of sampled correlators. *IEEE Trans Signal Proc* 1991;39:216–219.
- Parker KH, Jones CJ, Dawson JR, Gibson DG. What stops the flow of blood from the heart? *Heart Vessels* 1988;4:241–245.
- Reneman RS, van Merode T, Hick P, Muyltjens AM, Hoeks AP. Age-related changes in carotid artery wall properties in men. *Ultrasound Med Biol* 1986;12:465–471.
- Sindberg-Eriksen P, Gennser G, Lindstrom K, Benthin M, Dahl P. Pulse wave recording—development of a method for investigating foetal circulation in utero. *J Med Eng Technol* 1985;9:18–27.
- Sugawara M. Wave intensity analysis: a new method for the dynamic study of heart-vessel interactions. In: *Proc of the European medical and biological engineering conference, 1999, Vienna, Austria*. *Med Biol Eng Comp* 1999;37(Suppl 2):24–27.
- Tardy Y, Meister JJ, Perret F, Brunner HR, Arditi M. Non-invasive estimate of the mechanical properties of peripheral arteries from ultrasonic and photoplethysmographic measurements. *Clin Phys Physiol Meas* 1991;12:39–54.
- Torp H, Kristoffersen K. US5560363: Method for calculation of blood velocity and blood velocity spread from multigated Doppler signals. Assignee: Vingmed Sound A/S, Horten, Norway, 1995.